Wilkinson Microwave Anisotropy Probe (*WMAP*) Constraints on Non-Gaussianity

Eiichiro Komatsu for the WMAP science team [1]

Department of Astrophysical Sciences, Princeton University, Princeton, NJ 08540 (USA)

Abstract

The Wilkinson Microwave Anisotropy Probe (*WMAP*) has made it possible to test Gaussianity of fluctuations in the cosmic microwave background with unprecedented sensitivity, thanks to its careful instrumental design minimizing systematic errors. Constraints on the CMB non-Gaussianity offer a fundamental test of inflation and general relativistic perturbation theory. On the other hand, extragalactic radio sources produce significant non-Gaussian signals, making physical interpretations of the measured non-Gaussianity complex. Applying to the *WMAP* 1-year data a statistical tool we have developed for separately measuring the primordial and the source non-Gaussianities, we find: (1) CMB is consistent with Gaussian fluctuations, as predicted by inflation. The r.m.s. contribution from a second order (non-linear) term is smaller than 2×10^{-5} of the leading term. Note that the second-order perturbation theory predicts 10–100 times smaller value. (2) We have detected the source contribution at 41 GHz (Q band); thus, the *WMAP* map in Q band *is* weakly non-Gaussian at small angular scales because of the sources! This measurement has been used to determine the source contribution to the power spectrum in Q band. Our method can be applied to the Planck experiment, for which there is a chance to detect non-Gaussianity predicted by the second-order perturbation theory.

Key words: cosmic microwave background, cosmology: observations, early universe, gaussianity

---

[1] The WMAP science team: C. Barnes, C. Bennett (PI), M. Halpern, R. Hill, G. Hinshaw, N. Jarosik, A. Kogut, E. Komatsu, M. Limon, S. Meyer, N. Odegard, L. Page, H. Peiris, D. Spergel, G. Tucker, L. Verde, J. Weiland, E. Wollack, E. Wright

1 Introduction

The sky map of the cosmic microwave background (CMB) radiation is a picture of infant universe at $z \simeq 1089$, when the universe was 380,000 years old. (The universe would be only 1.5 days old then, if the universe were 137 years old today.) The Wilkinson Microwave Anisotropy Probe (*WMAP*) has recently produced clean and precise sky maps of the CMB in 5 microwave bands (Bennett et al., 2003a), with the angular resolution 30 times better than that of the Differential Microwave Radiometer (DMR) on board the Cosmic Background Explorer (*COBE*) (Bennett et al., 1996). Detailed study of these sky maps offers a fundamental test of cosmology, as various cosmological effects change temperature and energy distribution of the CMB at all angular scales (e.g. Hu & Sugiyama, 1995).

Statistical properties of fluctuations in the CMB are a powerful probe of cosmological models. The fluctuations are so tiny (10^{-5}) that the linear perturbation theory accurately describes the evolution of the fluctuations, given initial conditions and thermal history of the universe. As a result, theoretical predictions for the two-point statistics, such as the angular power spectrum of CMB temperature and polarization anisotropies, are accurate enough to compare with precise observations. The temperature and polarization power spectra of the *WMAP* data (Hinshaw et al., 2003a; Kogut et al., 2003) have determined the best-fit cosmological model with errors in the parameter determinations being quite small ($< 10\%$) (Spergel et al., 2003; Page et al., 2003b). The systematic errors in the parameter determinations are minimized by both the careful instrumental design (Hinshaw et al., 2003b; Jarosik et al., 2003; Page et al., 2003a; Barnes et al., 2003) and data analysis techniques (Verde et al., 2003). See also the contribution of L. Verde in this proceedings.

What else can we learn from the CMB sky? The angular power spectrum is not the only observable, if statistical properties of the CMB do not obey Gaussian statistics. Fluctuation fields are, in general, characterized by higher-order statistics such as the N-point correlation functions, the Minkowski functionals, the peak-peak correlation functions, etc., which are sensitive to deviation from Gaussianity, i.e., non-Gaussianity. Full understanding of the statistical properties of the CMB is also required for the detailed error analysis of the angular power spectrum. Physically, non-Gaussianity in the CMB should be closely associated with the origin of the fluctuations. Simple inflationary models based on a single scalar field predict Gaussian fluctuations as a consequence of the amplification of quantum fluctuations in a vacuum. (Non-Gaussianity is produced, but too small to detect; see Acquaviva et al. (2002); Maldacena (2002) for recent theoretical studies.) A single-field model provides an excellent fit to the angular power spectrum of the *WMAP* data (Peiris et al., 2003). More complex models with multiple fields or models that produce topological defects such as strings can produce stronger non-Gaussianity, but these models have to be consistent with the power spectrum measurements. The *COBE* DMR data has shown that the CMB is consistent with Gaussianity on large angular scales (e.g. Kogut et al., 1996; Komatsu et al., 2002). As we describe in this contribution, the *WMAP* data has extended the constraints down to sub-degree scales, finding no deviation from Gaussianity (Komatsu et al., 2003a). These results support simple inflationary models, but do not exclude possibilities of having a small contribution ($< 2 \times 10^{-5}$ in fraction) from non-Gaussian components.

If inflation does not produce significant non-Gaussianity, then the strongest source of cosmological non-Gaussianity in the CMB is the second-order perturbations in the gravitational potential (Luo & Schramm, 1993; Pyne & Carroll, 1996; Mollerach & Matarrese, 1997). This effect *must exist*, as long as the general relativistic perturbation theory is correct. The current theoretical estimate implies that the effect is 10–100 times smaller than our *WMAP* constraints. There is still a chance to detect the signal in future observations such as Planck (Komatsu et al., 2001), but we need more precise prediction for the form of non-Gaussianity in the gravitational potential.

Apart from the CMB, there are a number of non-cosmological, "foreground" sources in the microwave sky. The emission from our Galaxy is the brightest component, which must be masked or subtracted out before any cosmological analysis of the CMB. Since the *WMAP* observes in 5 frequency bands, much of the Galactic emission can be reliably subtracted using non-monochromatic nature of the Galaxy (Bennett et al., 2003b). The power spectra measured in different bands coincide with each other after the foreground subtraction, which is reassuring (Hinshaw et al., 2003a). Actually, much more problematic foreground component is the extragalactic radio sources. Although we can mask those positions of the sky which are known to have sources brighter than some threshold flux (which is determined by sensitivity of observations), there always remain undetected sources. The undetected (unmasked) sources potentially contaminate the cosmological CMB signals. Since we cannot subtract them out individually, we must estimate the effect of the sources in a statistical manner.

The emission from the sources is highly non-Gaussian and only important on small angular scales; thus, we can use the non-Gaussian signals to directly estimate the source contribution. This example illustrates usefulness of the higher-order statistics in a real life. In this contribution, we describe our approach to this problem and show results from the *WMAP* data.

2 Preparing the *WMAP* maps for the analysis

In this section, we describe step-by-step how to combine the *WMAP* maps available on the LAMBDA web site, in order to obtain a single map, $\bar{T}_i$, that was used for the analysis in Komatsu et al. (2003a) (the Q+V+W coadded map). The map is cleaned for the Galactic foreground emission. Also obtained is a map of the noise variance of $\bar{T}_i$, N_i.

(1) Download Q1,Q2,V1,V2,W1,W2,W3, and W4 map. The first column is the temperature data at pixel i, T_{ij}, in thermodynamic temperature, and the second column is the effective number of observations at pixel i, $N_{obs,ij}$, where $j = 1, 2, 3, ..., 8$ refers to Q1,Q2,V1,...,W4, respectively. Multiply the maps by 1000 to convert to μK.

(2) Calculate the weight, $w_{ij} = N_{obs,ij}/\sigma_{0,j}^2$, where $\sigma_{0,j}$ is given in Table 1 of Bennett et al. (2003a) or in "Description" at the download site.

(3) Calculate the noise variance at pixel i: $N_i = 1/(\sum_{j=1}^{8} w_{ij})$. This map will be used to calculate the inverse-noise-variance weight, N_i^{-1}, when measuring non-Gaussian signals from point sources.

(4) Download the foreground template maps, FDS ("Model dust map"), $H\alpha$ ("Composite all sky H-alpha"), and $Sync$ ("Haslam 408 MHz"), where FDS is the dust template at 94 GHz from Finkbeiner, Davis & Schlegel (1999), $H\alpha$ the free-free template from Finkbeiner (2003), and $Sync$ the synchrotron template from Haslam et al. (1981, 1982). Multiply FDS by 1000 to convert to μK in antenna temperature.

(5) Correct $H\alpha$ for extinction. Download the reddening template map, E_{B-V} ("Reddening"). Calculate a correction factor, $\xi = (1 - e^{-\tau})/\tau$, where $\tau = 2.2E_{B-V}$. (See section 3.1 of Bennett et al. (2003b).)

(6) Download the beam transfer functions, b_l^i, where $i = 1 - 8$ for Q1,...,W4.

(7) Smooth the foreground template maps with the beam, calculating

$$FDS(\hat{n}) = \sum_{lm} a_{lm}^{FDS} b_l^i Y_{lm}(\hat{n}), \tag{1}$$

$$H\alpha(\hat{n}) = \sum_{lm} a_{lm}^{H\alpha} b_l^i Y_{lm}(\hat{n}), \tag{2}$$

$$Sync(\hat{n}) = \sum_{lm} a_{lm}^{Sync} b_l^i Y_{lm}(\hat{n}), \tag{3}$$

where a_{lm} is the harmonic coefficients of the original template map.

(8) Subtract the best-fit foreground template maps using "an alternative fitting method" described in section 6 of Bennett et al. (2003b):

$$\begin{aligned}
\tilde{T}_Q &= T_Q - 1.044\,[1.036FDS + 1.923H\alpha/\xi + 1.006Sync] \\
\tilde{T}_V &= T_V - 1.100\left[0.619FDS + 1.923(\nu_V/\nu_Q)^{-2.15}H\alpha/\xi + 1.006(\nu_V/\nu_Q)^{-2.7}Sync\right] \\
\tilde{T}_W &= T_W - 1.251\left[0.873FDS + 1.923(\nu_W/\nu_Q)^{-2.15}H\alpha/\xi + 1.006(\nu_W/\nu_Q)^{-2.7}Sync\right]
\end{aligned}$$

where $\nu_Q = 40.7$ GHz, $\nu_V = 60.8$ GHz, and $\nu_W = 93.5$ GHz. The values in front of the left bracket convert the antenna temperature to the thermodynamic temperature. (See Table 1 of Bennett et al. (2003a).)

(9) Coadd the cleaned maps: $\bar{T}_i = \sum_{j=1}^{8} \tilde{T}_{ij} w_{ij} / (\sum_{j=1}^{8} w_{ij})$.

(10) Download the $Kp0$ Intensity Mask file.

(11) Apply the mask M_i (given in the second column of the file) to the coadded map, $\bar{T}_i \to \bar{T}_i M_i$. Removing monopole and dipole from the map (important!), we obtain the Q+V+W coadded map which can be used for testing Gaussianity!

3 Testing Gaussianity

3.1 Two Approaches

There are two approaches to testing Gaussianity of the CMB.

- Blind tests (null tests) which make no assumption about the form of non-Gaussianity. The simplest test would be measurements of deviation of one-point p.d.f. from a Gaussian distribution. (Measurements of skewness, kurtosis, etc., for example.) Being model-independent is a merit of this approach, while the statistical power is weak. If we had no models to test, this approach would be the only choice.
- Testing specific models of non-Gaussianity, constraining the model parameters. This approach is powerful in putting *quantitative* constraints on non-Gaussianity, at the cost of being model-dependent. If we had a sensible (yet fairly generic) model to test, this approach would be more powerful than the blind tests.

In what follows, we apply both approaches to the *WMAP* data.

3.2 The Minkowski Functionals

For the first test, we use the Minkowski functionals (Minkowski, 1903; Gott et al., 1990; Schmalzing & Górski, 1998), which measure morphological structures of the CMB, describing the properties of regions spatially bounded by a set of contours. The contours may be specified in terms of fixed temperature thresholds, $\nu = \Delta T/\sigma$, where σ is the standard deviation of the map, or in terms of the area. Parameterization of contours by threshold is computationally simpler, while parameterization by area reduces correlations between the Minkowski functionals (Shandarin et al., 2002). We use a joint analysis of the

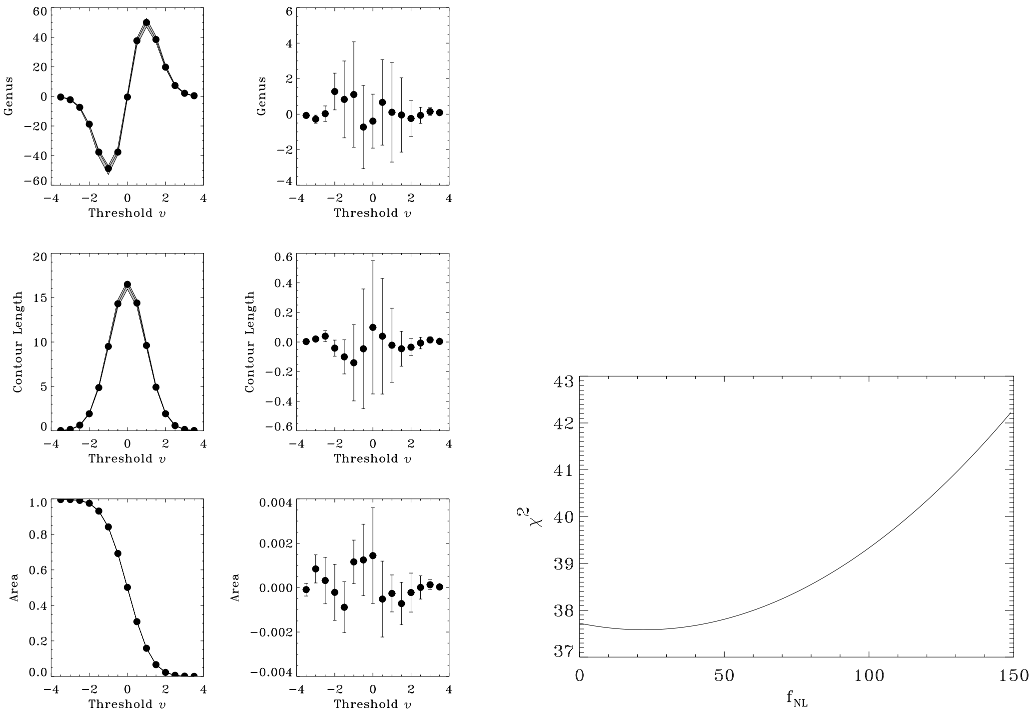

Fig. 1. (*Left Panel*) The Minkowski functionals for *WMAP* data (filled circles) at $28'$ pixel resolution, and the residuals between the mean of the Gaussian simulations and the *WMAP* data. The gray band shows the 68% confidence interval for the Gaussian Monte Carlo simulations. The *WMAP* data are in excellent agreement with the Gaussian simulations. (*Right Panel*) Limits to f_{NL} from χ^2 fit of the *WMAP* data to the non-Gaussian model. The fit is a joint analysis of the three Minkowski functionals shown in the left panel. There are 44 degrees of freedom.

three Minkowski functionals: (1) the total area above threshold, $A(\nu)$, (2) the total contour length, $C(\nu)$, and (3) the genus, $G(\nu)$, which is the number of hot spots minus the number of cold spots. We explicitly include their covariance; consequently, we work in the simpler threshold parameterization.

We have measured the Minkowski functionals at 5 different resolutions from the pixel size of 3.7 degrees in diameter to 12 arcminutes. Figure 1 shows one example at $28'$ pixel resolution. The gray band shows the 68% confidence region derived from 1000 Gaussian Monte Carlo simulations. (See section 2.3 of Komatsu et al. (2003a) for description of the simulations.) The *WMAP* data are in excellent agreement with the Gaussian simulations at all resolutions. But, *how Gaussian is it?*

For the second test, we use the "cubic" statistics (Komatsu, Spergel & Wandelt, 2003) which combine three-point (triangle) configurations of the angular bispectrum that are sensitive to the models under consideration. We call it "cubic", since the statistics consist of a cubic combination of temperature maps. (cf. The power spectrum is quadratic.) The cubic statistics have advantages of being easy to predict theoretically for a given model.

3.3.1 Primordial non-Gaussianity

We consider two components. The first one is the primordial non-Gaussianity parametrized by a non-linear coupling parameter, f_{NL} (Komatsu et al., 2001), which determines the amplitude of a quadratic term added to Bardeen's curvature perturbations, $\Phi(\mathbf{x}) = \Phi_L(\mathbf{x}) + f_{NL}\left[\Phi_L^2(\mathbf{x}) - \langle\Phi_L^2(\mathbf{x})\rangle\right]$, where Φ_L are Gaussian linear perturbations with zero mean. It is useful to estimate the r.m.s. amplitude of Φ to see how important the second-order term is. One obtains $\langle\Phi^2\rangle^{1/2} \simeq \langle\Phi_{\rm L}^2\rangle^{1/2}(1 + f_{\rm NL}^2\langle\Phi_{\rm L}^2\rangle)$, where $\langle\Phi^2\rangle^{1/2} \simeq 3.3\times10^{-5}$ (Bennett et al., 1996); thus, a fractional contribution from the second term is $f_{\rm NL}^2\langle\Phi_{\rm L}^2\rangle \simeq 10^{-5}(f_{NL}/100)^2$. We are talking about very small effects.

Although the form is inspired by simple inflation models, the exact predictions from those inflation models are irrelevant to our analysis here because the predicted amplitude of f_{NL} is much smaller than our sensitivity; however, this parameterization is useful to find *quantitative* constraints on the amount of non-Gaussianity allowed by the CMB data. Also, the form is general in that f_{NL} parameterizes the leading-order non-linear corrections to Φ. The second-order perturbation theory predicts $f_{NL} \sim 1 - 10$.

The model yields the bispectrum in the form of $B_{l_1l_2l_3} = f_{NL} I_{l_1l_2l_3} b^{prim}_{l_1l_2l_3}$, where

$$I_{l_1l_2l_3} \equiv \sqrt{\frac{(2l_1+1)(2l_2+1)(2l_3+1)}{4\pi}} \begin{pmatrix} l_1 & l_2 & l_3 \\ 0 & 0 & 0 \end{pmatrix}, \tag{4}$$

and

$$b^{prim}_{l_1l_2l_3} \equiv 2\int r^2 dr \left[\beta_{l_1}(r)\beta_{l_2}(r)\alpha_{l_3}(r) + (\text{two permutations})\right]. \tag{5}$$

The functions $\alpha_l(r)$ and $\beta_l(r)$ are defined by $\alpha_l(r) \equiv (2/\pi)\int k^2 dk g_{Tl}(k) j_l(kr)$, and $\beta_l(r) \equiv (2/\pi)\int k^2 dk P(k) g_{Tl}(k) j_l(kr)$, respectively, where r is the comoving distance, and $P(k)$ is the power spectrum of Φ. The radiation transfer function, $g_{Tl}(k)$, is related to the angular power spectrum as $C_l = (2/\pi)\int k^2 dk P(k) g_{Tl}^2(k)$.

Figure 2 shows f_{NL} measured from the Q+V+W coadded map using the cubic statistic, as a function of the maximum multipole l_{max}. (See Komatsu et al., 2003a, for details of measurements.) There is no significant detection of f_{NL} at any angular scale. There is no a significant band-to-band variation, or a significant detection in any band. The best constraint is $-58 < f_{NL} < 134$ (95%), or a fractional contribution to the r.m.s. of Φ from the second-order term is smaller than 2×10^{-5}. Note that f_{NL} for $l_{max} = 265$ has a smaller error than that for $l_{max} = 512$, because the latter is dominated by the instrumental noise. Since all the pixels outside the cut region are uniformly weighted, the inhomogeneous noise in the map (pixels on the ecliptic equator are noisier than those on the north and south poles) is not accounted for. This leads to a noisier estimator than a minimum variance estimator. The constraint on f_{NL} for $l_{max} = 512$ will improve with more appropriate pixel-weighting schemes (Heavens, 1998; Santos et al., 2003). The simple inverse noise (N^{-1}) weighting makes the constraints much worse than the uniform weighting, as it increases errors on large angular scales where the CMB signal dominates over the instrumental noise. (However, it works fine for the point sources.) The uniform weighting is thus closer to optimal.

The Minkowski functionals shown in Figure 1 also place constraints on f_{NL}, comparing the data to the predictions derived from Monte Carlo simulations of the non-Gaussian CMB. (See Appendix A of Komatsu et al., 2003a, for details of the simulations.) We find $f_{NL} < 139$ (95%), remarkably consistent with those obtained from the bispectrum.

3.3.2 Point-source non-Gaussianity

The second component is the foreground non-Gaussianity from radio point sources, parameterized by skewness, b_{src}. The angular bispectrum is given by $B_{l_1 l_2 l_3} = b_{src} I_{l_1 l_2 l_3}$. The filled circles in the right panels of Figure 2 show $b_{\rm src}$ measured in Q (top panel) and V (bottom panel) band. We have used source masks for various flux cuts, $S_{\rm c}$, defined at 4.85 GHz to make these measurements. (The masks are made from the GB6+PMN 5 GHz source catalogue.) We find that $b_{\rm src}$ increases as $S_{\rm c}$: the brighter sources unmasked, the more non-Gaussianity is detected. On the other hand one can make predictions for $b_{\rm src}$ using the source count model. Comparing the measured values of $b_{\rm src}$ with the predicted counts by Toffolatti et al. (1998) (dashed lines) at 44 GHz, one finds that the measured values are smaller than the predicted values by a factor of 0.65. The solid lines show the predictions multiplied by 0.65. Our value for the correction factor matches well the one obtained from the *WMAP* source counts for $2 - 10$ Jy in Q band (Bennett et al., 2003b).

The source bispectrum, b_{src}, is related to the source power spectrum, c_{src}, by

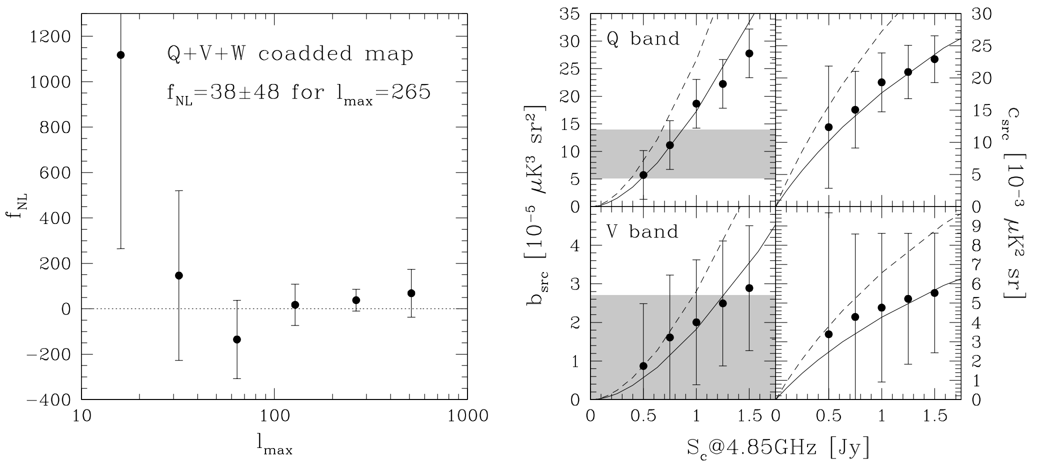

Fig. 2. (*Left Panel*) The non-linear coupling parameter, f_{NL}, as a function of the maximum multipole l_{max}, measured from the Q+V+W coadded map using the bispectrum estimator. The error bars at each l_{max} are not independent. (*Right Panel*) The point-source angular bispectrum b_{src} and power spectrum c_{src}. The left panels show b_{src} in Q band (top panel) and V band (bottom panel). The shaded areas show measurements from the *WMAP* sky maps with the standard source cut, while the filled circles show those with flux thresholds S_c defined at 4.85 GHz. The dashed lines show predictions from the source count model of Toffolatti et al. (1998), while the solid lines are those multiplied by 0.65 to match the *WMAP* measurements. The right panels show c_{src}. The filled circles are computed from the measured b_{src} substituted into equation (6). The lines are predictions. The error bars are not independent.

an integral relation (Komatsu et al., 2003a),

$$c_{src}(S_c) = b_{src}(S_c)[g(\nu)S_c]^{-1} + \int_0^{S_c} \frac{dS}{S} b_{src}(S)[g(\nu)S]^{-1}, \tag{6}$$

where $g(\nu)$ is a conversion factor from Jy sr^{-1} to μK which depends on observing frequency ν as $g(\nu) = (24.76 \text{ Jy } \mu\text{K}^{-1} \text{ sr}^{-1})^{-1}[(\sinh x/2)/x^2]^2$, $x \equiv h\nu/k_{\rm B}T_0 \simeq \nu/(56.78 \text{ GHz})$. We can use this equation combined with the measured b_{src} as a function of the flux threshold S_c to directly determine c_{src} as a function of S_c, *without relying on any extrapolations*. The right panels of Figure 2 also show the estimated $c_{\rm src}$ as filled circles. The measurements suggest that $c_{\rm src}$ for the standard source mask (indicated by the shaded area) is $c_{\rm src} = (15{\pm}6){\times}10^{-3}\ \mu\text{K}^2$ sr in Q band. In V band, $c_{\rm src} = (4.5{\pm}4){\times}10^{-3}\ \mu\text{K}^2$ sr.

In addition to the bispectrum, we have carried out other different methods to estimate the source contribution: (1) extrapolation from the number counts of detected sources in the *WMAP* data (Bennett et al., 2003b), and (2) the angular power spectrum on small angular scales (Hinshaw et al., 2003a). These methods yield consistent results.

4 Discussion

The *WMAP* 1-year data has enormously improved sensitivity for testing Gaussianity of the CMB. Yet, we do not have any compelling evidence for the cosmological non-Gaussianity. This result is consistent with what is predicted by inflation and the second-order perturbation theory. There may be a chance to find non-Gaussian signals from the second-order perturbations, which predict $f_{NL} \sim 1 - 10$. (The current theoretical predictions do not have an accuracy better than this.) Detection can be made possible by the Planck experiment combining the temperature and polarization anisotropies. While we can detect $f_{NL} \sim 5$ by using the temperature alone (Komatsu et al., 2001), combining the polarization measurements increases our sensitivity: we have several observables for the bispectrum such as $\langle TTT \rangle$, $\langle TTE \rangle$, $\langle TEE \rangle$, and $\langle EEE \rangle$. The future polarization-dedicated satellite experiment (e.g., CMBPol) in combination with the Planck temperature map may enable us to detect $f_{NL} \sim 3$.

We have shown usefulness of the angular bispectrum as an estimator of the point-source contributions. Any experiments that are potentially contaminated by the sources should use the bispectrum to accurately characterize the effects of the sources.

The *WMAP* mission is made possible by the support of the Office of Space Sciences at NASA Headquarters and by the hard and capable work of scores of scientists, engineers, technicians, machinists, data analysts, budget analysts, managers, administrative staff, and reviewers.

References

V. Acquaviva, N. Bartolo, S. Matarrese, & A. Riotto, 2002, preprint (astro-ph/0209156)
C. Barnes et al. 2003, ApJ, in press (astro-ph/0302215)
C. L. Bennett et al. 1996, ApJ, 464, 1
C. L. Bennett et al. 2003a, ApJ, in press (astro-ph/0302207)
C. L. Bennett et al. 2003b, ApJ, in press (astro-ph/0302208)
D. P. Finkbeiner, 2003, ApJS, in press (astro-ph/0301558)
D. P. Finkbeiner, M. Davis, D. J. Schlegel, 1999, ApJ, 544, 81
J. R. Gott, C. Park, R. Juszkiewicz, W. E. Bies, D. P. Bennett, F. R. Bouchet, & A. Stebbins, 1990, ApJ, 352, 1
C. G. T. Haslam, U. Klein, C. J. Salter, H. Stoffel, E. W. Wilson, M. N. Cleary, D. J. Cooke, & P. Thomasson, 1981, A&A, 100, 209

C. G. T. Haslam, H. Stoffel, C. J. Salter, E. W. Wilson, 1982, A&AS, 47, 1
A. F. Heavens, 1998, MNRAS, 299, 805
G. Hinshaw et al. 2003a, ApJ, in press (astro-ph/0302217)
G. Hinshaw et al. 2003b, ApJ, in press (astro-ph/0302222)
W. Hu, & N. Sugiyama, 1995, ApJ, 444, 489
N. Jarosik et al. 2003, ApJ, in press (astro-ph/0302224)
A. Kogut et al. 1996, ApJ, 464, 29
A. Kogut et al. 2003, ApJ, in press (astro-ph/0302213)
E. Komatsu, & D. N. Spergel, 2001, PRD, 63, 063002
E. Komatsu, B. D. Wandelt, D. N. Spergel, A. J. Banday, & K. M. Górski, 2002, ApJ, 566, 19
E. Komatsu et al. 2003, ApJ, in press (astro-ph/0302223)
E. Komatsu, D. N. Spergel, & B. D. Wandelt, 2003, ApJ, submitted (astro-ph/0305189)
X. Luo, & D. Schramm, 1993, PRL, 71, 1124
J. Maldacena, 2002, preprint (astro-ph/0210603)
H. Minkowski, 1903, Mathematische Annalen, 57, 447
S. Mollerach, & S. Matarrese, 1997, PRD, 56, 4494
L. Page et al. 2003a, ApJ, in press (astro-ph/0302214)
L. Page et al. 2003b, ApJ, in press (astro-ph/0302220)
H. Peiris et al. 2003, ApJ, in press (astro-ph/0302225)
T. Pyne, & S. M. Carroll, 1996, PRD, 53, 2920
M. G. Santos et al. 2003, MNRAS, 341, 623
J. Schmalzing, & K. M. Górski, 1998, MNRAS, 297, 355
S. F. Shandarin, H. A. Feldman, Y. Xu, & M. Tegmark, 2002, ApJS, 141, 1
D. N. Spergel et al. 2003, ApJ, in press (astro-ph/0302209)
L. Toffolatti, G. F. Argueso, G. de Zotti, P. Mazzei, A. Franceschini, L. Danese, & C. Burigana, 1998, MNRAS, 297, 117
L. Verde et al. 2003, ApJ, in press (astro-ph/0302218)